Research Article | Vol. 26, No. 16 | 6 Aug 2018 | OPTICS EXPRESS 21210
Optics EXPRESS

# Multiple-plane image formation by Walsh zone plates

FEDERICO MACHADO,[1] VICENTE FERRANDO,[1] FERNANDO GIMÉNEZ,[2] WALTER D. FURLAN,[3] AND JUAN A. MONSORIU[1,*]

[1]Centro de Tecnologías Físicas, Universidad Politécnica de Valencia, E-46022, Valencia, Spain
[2]Instituto de Matemática Pura y Aplicada, Universidad Politécnica de Valencia, E-46022, Valencia, Spain
[3]Departamento de Óptica, Universitat de València, Burjassot, E-46100, Spain
[*]jmonsori@fis.upv.es

**Abstract:** A radial Walsh filter is a phase binary diffractive optical element characterized by a set of concentric rings that take the phase values 0 or π, corresponding to the values + 1 or −1 of a given radial Walsh function. Therefore, a Walsh filter can be re-interpreted as an aperiodic multifocal zone plate, capable to produce images of multiple planes simultaneously in a single output plane of an image forming system. In this paper, we experimentally demonstrate for the first time the focusing capabilities of these structures. Additionally, we report the first achievement of images of multiple-plane objects in a single image plane with these aperiodic diffractive lenses.



## 1. Introduction

Fresnel zone plates (FZPs) are essential for focusing and imaging in many scientific and technological areas, as for example in THz [1] or X-Ray [2] applications. As it is well-known, conventional FZPs consist of alternating transparent-opaque circular rings (or alternating 0 and π phase shift ring zones) whose radii are proportional to the square root of the natural numbers [3]. Therefore, as these lenses have rotational symmetry, their complex transmittance function can be, in general, formulated in terms of a one-dimensional compact-supported periodic function $q(\varsigma)$, followed by a change of coordinates $\varsigma = (r/a)^2$, where $r$ is the radial coordinate and $a$ the radius of the lens. In order to extend the range of applications of conventional FZPs several non-linear transformations of the phase of periodic zone plates were proposed, mainly to obtain multifocal zone plates [4–6]. On the other hand, several diffractive lenses characterized by non-periodic or aperiodic generators, $q(\varsigma)$ were also proposed over the last ten years. For instance, Fractal Zone Plates [7–9] (characterized by its fractal structure along the squared radial coordinate $\varsigma$) demonstrated self-similar focusing properties [7] and extended depth of field imaging [8]. Other interesting aperiodic functions are the Fibonacci and Thue-Morse sequences [10]. Fibonacci zone plates are intrinsically bifocals, being the ratio of the two main focal distances defined by the golden ratio [11]. Thue-Morse zone plates combine the properties of fractal and Fibonacci zone plates producing two main self-similar foci along the optical axis with extended depth of focus [12].

Walsh functions are a set piecewise constant functions satisfying orthogonality conditions over the unit interval [13]. These functions take values + 1 and −1 on sub-intervals defined by dyadic fractions, being the number of zero crossings determined by the order of the Walsh function. Walsh functions are of great practical interest in many fields, especially in communications [14] and digital signal processing [15]. Derived from Walsh functions in polar coordinates, radial Walsh filters (structures with rotational symmetry) have been proposed for solving problems of optical science. For example, these filters have been proved to be useful in adaptive optics and apodization problems [16, 17], and for tailoring the resolution of microscopic systems [18]. Earlier studies on radial Walsh filters have shown that

#331211 https://doi.org/10.1364/OE.26.021210
Journal © 2018 Received 9 May 2018; revised 8 Jul 2018; accepted 23 Jul 2018; published 2 Aug 2018

Optics EXPRESS

the corresponding axial and transverse intensity distributions in the far-field diffraction patterns present self-similar properties [19, 20].

In this work, radial Walsh filters are re-interpreted as members of the above mentioned aperiodic zone plates family. In this way, a new formulation of a Walsh Zone Plate (WZP) is obtained by replacing the generating function $q(\varsigma)$, by a given Walsh function with a fixed number of zones. To evaluate the focusing and imaging properties of the WZPs two different optical setups were implemented. One of them uses a spatial light modulator to obtain the axial irradiance provided by quadrifocal WZP and to perform the first image formation experiment with phase WZPs. In the other one, we demonstrate that amplitude WZPs are capable of achieving images of multiple-plane object in a single image plane.

## 2. Walsh zone plates design and focusing properties

Let us start revising the concept of radial Walsh filters [19, 20]. It was based on the Walsh functions represented in Fig. 1. The first step in the construction procedure consists of representing the binary decomposition of an integer number $k$ in the form:

$$k = \sum_{i=0}^{m-1} k_i 2^i, \tag{1}$$

where $k_i$ is the $i$-th bit, 0 or 1, of the binary numeral for $k$ and $m$ is the lowest integer number for which $2^m > k$, i.e., $2^m$ is the power of 2 that exceeds $k$. Based on this decomposition, the corresponding Walsh function of order $k$, $q_k(\varsigma)$, can be defined in the interval $\varsigma \in [0,1]$ as:

$$q_k(\varsigma) = \prod_{i=0}^{m-1} \operatorname{sgn}\left[\cos\left(\pi 2^i k_i \varsigma\right)\right]. \tag{2}$$

The function $\operatorname{sgn}[x]$ is defined as:

$$\operatorname{sgn}[x] = \begin{cases} +1, & x > 0 \\ 0, & x = 0 \\ -1, & x < 0 \end{cases}. \tag{3}$$

In Fig. 1 we have represented the Walsh functions, $q_k(\varsigma)$, up to order $k = 64$. The yellow bars correspond to the value + 1 while the red bars correspond to the value –1. Note that the number of zero crossings is determined by the order of the Walsh function $k$.

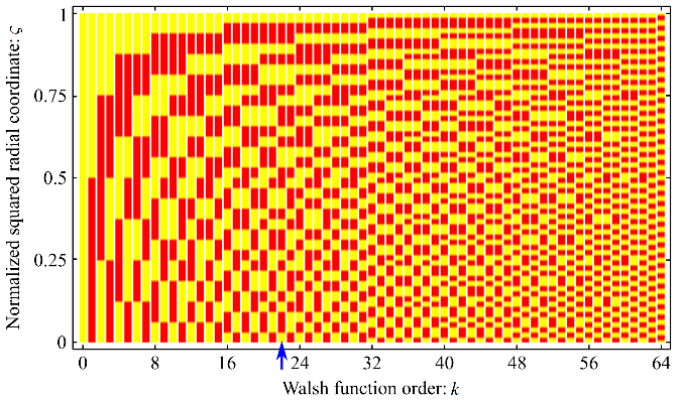


Fig. 1. Graphical representation of the Walsh functions up to order $k = 64$. The yellow bars correspond to the value + 1 while the red bars correspond to the value –1. The blue arrow indicates the order $k = 22$, which has been used to design the WZP shown in Fig. 2.

Optics EXPRESS

From a particular Walsh function, $q_k(\varsigma)$, the corresponding radial Walsh filter can be generated by performing a change of variable $\varsigma = (r/a)^2$ and by rotating the transformed Walsh function around ones of its extremes. The result is a pure phase diffractive optical element having a radial coordinate $r$ and radius $a$. In this way, we can re-interpret a radial Walsh filter of order $k$ as a binary phase aperiodic zone plate whose pupil function is defined by the Walsh function, $q_k(\varsigma)$, expressed in the normalized squared radial coordinate $\varsigma$.

Figure 2(a) shows a WZP of order $k = 22$ characterized by a set of concentric zones that take the phase values 0 (yellow rings) or $\pi$ (red rings), corresponding to transmittance values + 1 or –1, respectively. For comparison, a conventional phase binary zone plate with the same resolution (same width of the outermost zone) is also represented in the same figure. Note that this FZP can be obtained using the same procedure but by replacing the aperiodic Walsh function with a periodic one (i.e., a sequence of alternating zones in opposite phase). In other words, a WZP can be understood as a binary FZP, where the positions of some zones of equal-area have been interchanged.

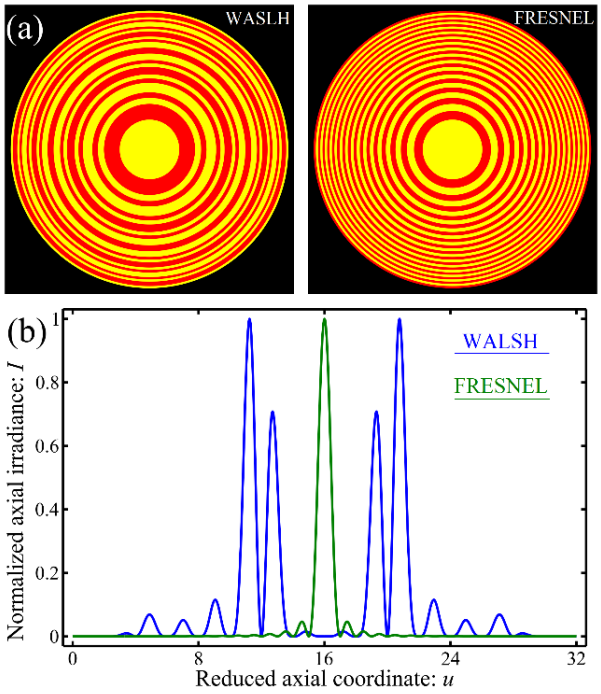


Fig. 2. (a) WZP generated from the 1-D function $q_{22}(\varsigma)$ shown in Fig. 1 and a FZP with the same number of Fresnel zones. Yellow and red rings correspond to a phase 0 ( + 1 transmittance value) and $\pi$ (–1 transmittance value), respectively. (b) Numerically computed axial irradiance produced by both lenses shown against the reduced axial coordinate $u$.

The focusing properties of the WZPs can be evaluated by computing the axial irradiance generated by these aperiodic lenses under monochromatic plane-wave illumination. To this end, we have employed the mathematical basis provided by the McCutchen theorem [21], which relates (via 1-D Fourier transform) the axial irradiance distribution with certain representations of the pupil function [22,23]. In our case, the axial irradiance function is given by

$$I(u) = 4\pi^2 u^2 \left| \int_0^1 q(\zeta) \exp\left(-i2\pi u \zeta\right) d\zeta \right|^2 , \qquad (4)$$

Optics EXPRESS

where $u = a^2/2\lambda z$ is the reduced axial coordinate, $z$ is the axial distance from the pupil plane, and $\lambda$ is the wavelength of the light. Thus, the axial irradiance can be defined in terms of the Fourier transform of the mapped pupil function $q(\varsigma)$.

By using Eq. (4) we have computed the axial irradiance (corresponding to the first-order diffraction foci) provided by both: a WZP of order $k = 22$, and by a FZP with the same number of Fresnel zones, for comparison. The result shown in Fig. 2(b) proves that the reordering of the phase zones according to the aperiodic Walsh function produces a multiple splitting of the first-order focus of the corresponding FZP (see the green line in Fig. 2) generating, in our case, four foci along the axial coordinate (see the blue line in Fig. 2). Therefore, Walsh functions can be implemented in the design of novel multifocal diffractive lenses with multi-imaging capabilities. Due to the binary nature of the diffraction structure, other foci corresponding to positive high diffraction orders are also generated (not shown in Fig. 2 because of the represented range of axial coordinate), so these four foci are replicated along the reduced axial coordinate $u$ with a period corresponding to the number of zones, $N$.

We have also computed in Fig. 3 the axial irradiance of WZPs for different orders, $k$. For comparison, the normalized reduced axial coordinate, $u' = u/N$, has been considered, focusing our attention around the first diffraction order. The gray-code bars give the normalized axial irradiance, $I$, of theses diffractive aperiodic lenses, being $I = 1$ in the white regions and $I = 0$ in the black regions. First, we can easily identify the four foci shown in Fig. 2(b) in the irradiance bar in Fig. 3 for $k = 22$. Note that the four focal distances can be modulated with the parameter $k$. It is also shown that this quadrifocal configuration is preserved for different orders $k$, although more subsidiary foci appear for large $k$ values. It can also be seen that the four foci collapse to a single focus for $k = 1, 3, 7, 15, 31, 63, \ldots = 2^n\text{-}1$ with $n = 1, 2, 3, 4\ldots$since the structure of the corresponding WZP matches with a conventional periodic zone plate.

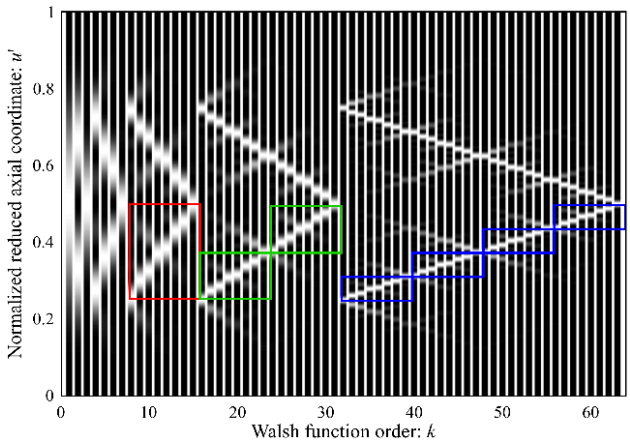


Fig. 3. The grey-code bars represent the normalized axial irradiances, $I$, for WZPs of different orders $k$, being $I = 1$ in the white regions and $I = 0$ in the black regions. The reduced axial coordinate has been normalized to $u' = u/N$, where $N$ is the number of zones. The red, green and blue boxes show the same structure at different scales.

On the other hand, the irradiances produced by WZPs under monochromatic plane-wave illumination present self-similar properties. For instance, the irradiances shown in the red box for $8 \le k \le 15$ are replicated on a smaller scale in the two green boxes for $16 \le k \le 31$ and even on smaller scale in the four blue boxes for $32 \le k \le 63$. The property of self-similarity in axial intensity distributions of radial Walsh filters was also reported in the far field diffraction patterns [20]. We have extended this property to the axial irradiances provided by WZPs working as aperiodic diffractive lenses.

Optics EXPRESS

### 3. Experimental results: imaging properties

We have experimentally tested the focusing and multi-imaging capabilities of aperiodic WZPs and compared their performance against a conventional FZP with the same number of Fresnel zones. A schematic illustration of the experimental setup is shown in Fig. 4(a). The diffractive lenses under study were implemented on a Liquid Crystal in a Silicon SLM (Holoeye PLUTO with 8-bit gray-level corresponding to $2^8$ phase levels, a pixel size of 8 μm, and a resolution equal to 1920 × 1080 pixels). The SLM operating in phase-only modulation mode was calibrated for a 2π phase shift at $\lambda$ = 633 nm. In order to avoid the noise originated from the specular reflection (zero order diffraction) and from the higher diffraction orders due to the pixelated structure of the SLM, a 1D blazed grating acting as a linear phase carrier was also modulated on the SLM in addition to the WZP phase profile. This linear phase was compensated by tilting the SLM and by using a pin-hole (PH) to filter all diffraction orders except the first one into the focal plane of lens L2. In this way, a rescaled image of the diffractive lens was achieved at the L3 lens focal plane (exit pupil).

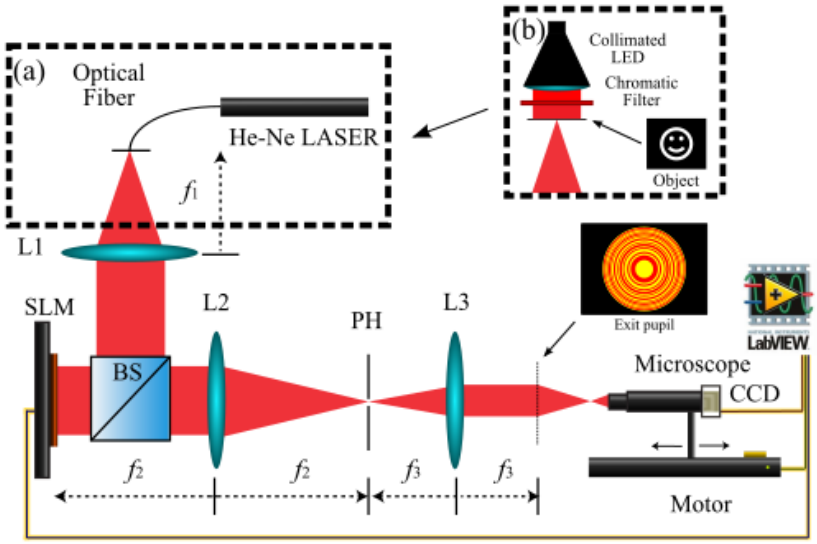


Fig. 4. Experimental setup for the assessment of (a) the multi-focusing properties of WZPs and (b) the multi-imaging capabilities by replacing the laser light source by a monochromatic LED illuminating a binary object (a smiley face).

A collimated beam from a He-Ne laser ($\lambda$ = 633nm) was directed onto the SLM. The diffracted field was captured and registered with a microscope (4x Zeiss Plan-Apochromat objective) attached to a CCD camera (8 bit gray-level with a pixel pitch of 3.75 μm and 1280 × 960 pixels). The microscope and the CCD were mounted on a translation stage (Thorlabs LTS 300 with a range of 300 mm and a precision of 5μm) along the optical axis. The experimental irradiances obtained for a WZP of order $k$ = 22 and radius $a$ = 1.74 mm is shown in Fig. 5(a). A profile of the measured axial irradiance is represented in Fig. 5(b), together with the results numerically computed using Eq. (4). A very good agreement between theory and experiment can be observed and the four foci marked with the characters [A-D] are clearly visible. The corresponding focal distances were $f_A$ = 114.9 mm, $f_B$ = 124.8 mm, $f_C$ = 188.2 mm, and $f_D$ = 211.7 mm. Note in both cases, the heights of the different foci peaks and the transverse resolution at each focus are different. To quantify these differences we have computed the ratio of the full width at half-maximum (FWHM) of the axial irradiance peaks provided by the WZP and the corresponding FZP with the same number of zones. The results are shown in Table 1.

Optics EXPRESS

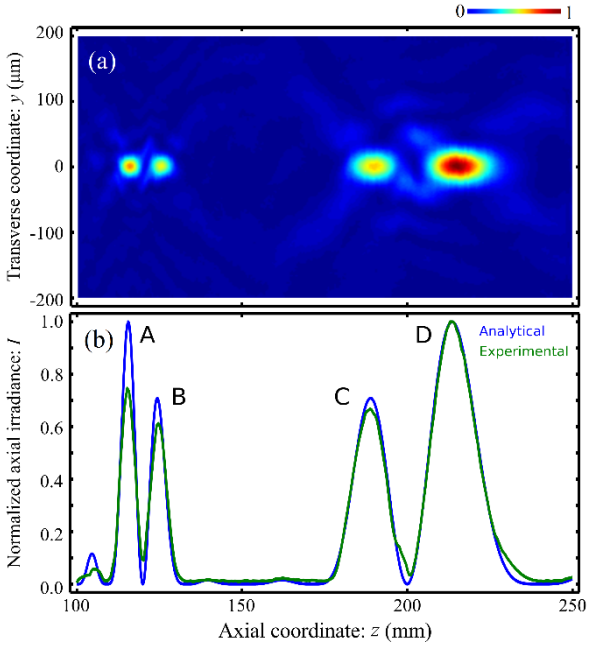


Fig. 5. (a) Experimental transverse intensity distribution produced by a WZP of order $k = 22$. (b) Profile of Fig. 5(a) (blue line) showing the axial irradiance distribution. The theoretical values of the irradiance are shown in green line for comparison. In both cases, the values are normalized to the peak intensity.

**Table 1. Ratios of the full width at half-maximum (FWHM) of the axial irradiance peaks provided by the WZP and the corresponding FZP with the same number of zones. A, B, C, and D correspond to the peaks shown in Fig. 5.**

| | WZP A/ FZP | WZP B/ FZP | WZP C/ FZP | WZP D/ FZP |
|---|---|---|---|---|
| **FWHM ratios** | 0.84 | 0.92 | 1.23 | 1.39 |

In order to verify the multi-imaging capabilities of WZPs we have modified the previous experimental setup as shown in Fig. 4(b). We replaced the He-Ne laser source by a binary object (a smiley face) located at the focal plane of the achromatic Badal lens, L1. The illumination system consisted of a red collimated LED (Mounted High-Power LED, red 625 nm, 1000 mA) and a bandpass filter ($\lambda = 632.8$ nm $\pm$ 0.6 nm). The multiple images produced by the aperiodic diffractive lens were captured with same image registration system (the CCD camera mounted on the translation stage). Figure 6 shows the images provided by the multifocal WZP of order $k = 22$ and the monofocal FZP shown in Fig. 2(a). The experimental results were reproduced without any post-processing. The registered images were obtained at each focal plane that can be tuned by a proper selection of the parameter $k$. As can be seen, four clear images were captured at the focal planes [A-D] depicted in Fig. 5(b), demonstrating in this way the multiple-plane imaging capabilities of the WZP as quadrifocal diffractive lens. For comparison, the four images obtained through WZP and the one with FZP are shown in the same figure. The image provided by the FZP has higher contrast than those provided by the WZP because all the images are coaxial and therefore in each case three out-of-focus images are superimposed to the in-focus image.

Optics EXPRESS

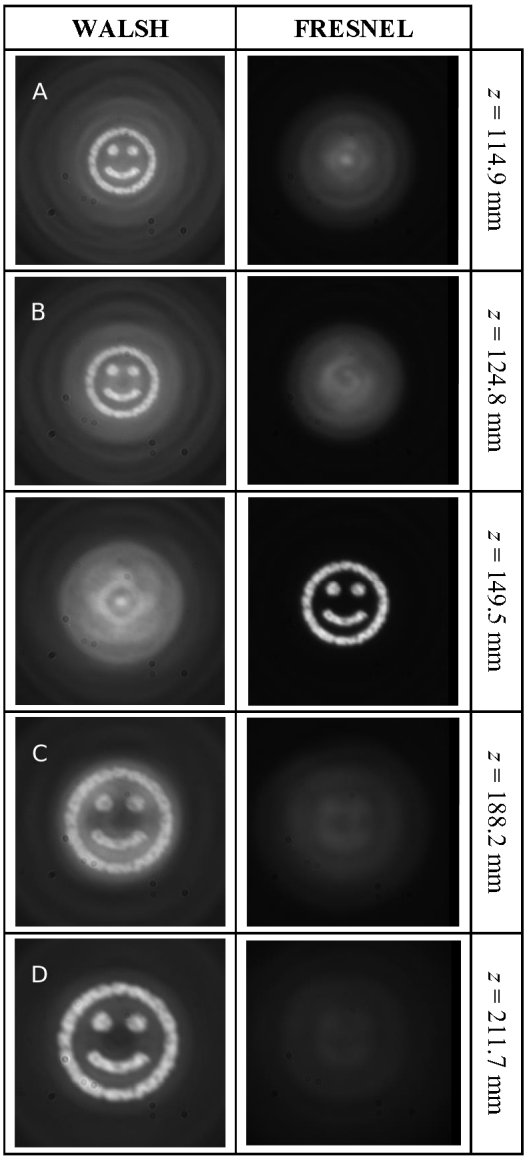


Fig. 6. (6.15 Mb) Images obtained with the WZP of order $k$ = 22 and with the equivalent periodic zone plate of the same resolution (see Visualization 1). Five different location, $z$, were considered corresponding to the four image planes of the quadrifocal WZP (first, second, fourth and fifth rows) and the image plane of the monofocal FZP (third row).

We have also tested the performance of amplitude WZPs as multifocal lenses by imaging objects located at different distances from the lens on a single image plane. For this purpose, we have implemented the experimental setup shown in Fig. 7(a). A WZP of order $k$ = 22 and radius $a$ = 3 mm (but in this case with opaque and transparent areas) was printed on a graphic film (standard polyester film) using a photoplotter with 2400 lpi resolution. The A binary amplitude object (our group logo: DiOG) was placed in front of a Badal Lens ($L_B$), to generate different object vergences. The WZP was located at the focal plane of $L_B$ in order to obtain the four images of the object at the focal plane of the lens $L_F$ all with the same size. The four images provided by the first diffraction order of the WZP at different vergences are shown in Fig. 7(b).

Optics EXPRESS

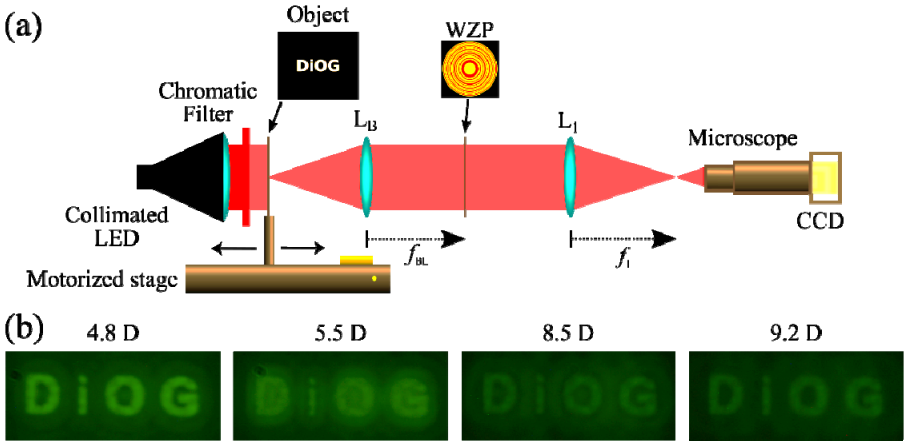


Fig. 7. (a) Experimental setup used to obtain images of different axially displaced objects at the same image plane. (b) Experimental results obtained with an amplitude WZP of order $k$ = 22. The position of the object is given in diopters.

## 4. Conclusions

In this work we have experimentally demonstrated, for the first time to our knowledge, the multiple-plane imaging and focusing capability of WZPs. First, we have shown that a WZP naturally produces multiple foci along the axial coordinate. A very good agreement between the experimental and the theoretical results has been obtained. Then, the images produced by these kind of filters working as quadrifocal diffractive lenses are reported. As the axial separation between the foci can be tuned by a proper selection of the Walsh order, $k$, these lenses offer a versatile alternative that can be advantageously used in several potential applications, as for instance, multiple plane optical trapping [24], X-ray microscopy [25], and multifocal contact and intraocular lenses [26–28].

## Funding

Ministerio de Economía y Competitividad and FEDER (DPI2015-71256-R); Generalitat Valenciana (PROMETEO II-2014-072); MayaNet - Erasmus Mundus Partnership 552061-EM-1-2014-1-IT-ERA MUNDUS-EMA21 (2014-0872/001-001).

## References

1. X. Wang, Z. Xie, W. Sun, S. Feng, Y. Cui, J. Ye, and Y. Zhang, "Focusing and imaging of a virtual all-optical tunable terahertz Fresnel zone plate," Opt. Lett. **38**(22), 4731–4734 (2013).
2. I. Mohacsi, I. Vartiainen, B. Rösner, M. Guizar-Sicairos, V. A. Guzenko, I. McNulty, R. Winarski, M. V. Holt, and C. David, "Interlaced zone plate optics for hard X-ray imaging in the 10 nm range," Sci. Rep. **7**(1), 43624 (2017).
3. J. Ojeda-Castañeda and C. Gómez-Reino, eds., *Selected Papers on Zone Plates* (SPIE Optical Engineering, 1996).
4. V. A. Soifer, V. V. Kotlyar, and L. L. Doskolovich, Iterative Methods for Diffractive Optical Elements Computation (Taylor & Francis, 1997).
5. M. A. Golub, L. L. Doskolovich, N. L. Kazanskiy, S. I. Kharitonov, and V. A. Soifer, "Computer generated diffractive multi-focal lens," J. Mod. Opt. **39**(6), 1245–1251 (1992).
6. L. L. Doskolovich, E. A. Bezus, A. A. Morozov, V. Osipov, J. S. Wolffsohn, and B. Chichkov, "Multifocal diffractive lens generating several fixed foci at different design wavelengths," Opt. Express **26**(4), 4698–4709 (2018).
7. G. Saavedra, W. D. Furlan, and J. A. Monsoriu, "Fractal zone plates," Opt. Lett. **28**(12), 971–973 (2003).
8. J. Monsoriu, G. Saavedra, and W. Furlan, "Fractal zone plates with variable lacunarity," Opt. Express **12**(18), 4227–4234 (2004).
9. W. D. Furlan, G. Saavedra, and J. A. Monsoriu, "White-light imaging with fractal zone plates," Opt. Lett. **32**(15), 2109–2111 (2007).
10. E. Maciá, "The role of aperiodic order in science and technology," Rep. Prog. Phys. **69**(2), 397–441 (2006).

Optics EXPRESS


11. J. A. Monsoriu, A. Calatayud, L. Remon, W. D. Furlan, G. Saavedra, and P. Andrés, "Bifocal Fibonacci diffractive lenses," IEEE Photonics J. **5**(3), 3400106 (2013).
12. V. Ferrando, F. Giménez, W. D. Furlan, and J. A. Monsoriu, "Bifractal focusing and imaging properties of Thue-Morse Zone Plates," Opt. Express **23**(15), 19846–19853 (2015).
13. J. L. Walsh, "A closed set of normal orthogonal functions," Am. J. Math. **45**(1), 5–24 (1923).
14. H. F. Harmuth, "Applications of Walsh functions in communications," IEEE Spectr. **6**(11), 82–91 (1969).
15. K. G. Beauchamp, *Applications of Walsh and related functions* (Academic Press, London, 1984).
16. L. N. Hazra, "A new class of optimum amplitude filters," Opt. Commun. **21**(2), 232–236 (1977).
17. L. N. Hazra and A. Banerjee, "Applications of Walsh functions in generation of optimum apodizers," J. Opt. **5**, 19–26 (1976).
18. L. N. Hazra, "Walsh filters for tailoring of resolution in microscopic imaging," Micron **38**(2), 129–135 (2007).
19. P. Mukherjee and L. N. Hazra, "Self-similarity in radial Walsh filters and axial intensity distributions in the far-field diffraction pattern," J. Opt. Soc. Am. A **31**(2), 379–387 (2014).
20. P. Mukherjee and L. N. Hazra, "Self-similarity in transverse intensity distributions in farfield diffraction patterns of radial Walsh filters," Adv. Opt. **2014**, 352316 (2014).
21. C. W. McCutchen, "Generalized aperture and the three-dimensional diffraction image," J. Opt. Soc. Am. **54**(2), 240 (1964).
22. J. Ojeda-Castañeda and L. R. Berriel-Valdos, "Zone plate for arbitrarily high focal depth," Appl. Opt. **29**(7), 994–997 (1990).
23. L. Ledesma-Carrillo, C. M. Gómez-Sarabia, M. Torres-Cisneros, R. Guzmán-Cabrera, C. Guzmán-Cano, and J. Ojeda-Castañeda, "Hadamard circular masks: high focal depth with high throughput," Opt. Express **25**(15), 17004–17020 (2017).
24. W. D. Furlan, F. Gimenez, A. Calatayud, L. Remon, and J. A. Monsoriu, "Volumetric multiple optical traps produced by Devil's lenses," J. Eur. Opt. Soc. Rap. Pub. **5**, 10037s (2010).
25. D. Wu, L. G. Niu, Q. D. Chen, R. Wang, and H. B. Sun, "High efficiency multilevel phase-type fractal zone plates," Opt. Lett. **33**(24), 2913–2915 (2008).
26. P. Valle, J. Oti, V. Canales, and M. Cagigal, "Visual axial PSF of diffractive trifocal lenses," Opt. Express **13**(7), 2782–2792 (2005).
27. V. Osipov, L. L. Doskolovich, E. A. Bezus, T. Drew, K. Zhou, K. Sawalha, G. Swadener, and J. S. W. Wolffsohn, "Application of nanoimprinting technique for fabrication of trifocal diffractive lens with sine-like radial profile," J. Biomed. Opt. **20**(2), 025008 (2015).
28. U. Hinze, A. El-Tamer, L. L. Doskolovich, E. A. Bezus, S. Reiß, H. Stolz, R. F. Guthoff, O. Stachs, and B. Chichkov, "Additive manufacturing of a trifocal diffractive-refractive lens," Opt. Commun. **372**, 235–240 (2016).